Journal of Alloys and Compounds 489 (2010) 689–693

Contents lists available at ScienceDirect

Journal of Alloys and Compounds

journal homepage: www.elsevier.com/locate/jallcom

Preparation and characteristics of yellow ZnS:Mn,Ce phosphor

Su-Hua Yang[a,*], Yu-Jiu Lial[b], Nai-Jen Cheng[b], Yin-Hsuan Ling[a]

[a] Department of Electronic Engineering, National Kaohsiung University of Applied Sciences, 415 Chien Kung Road, Kaohsiung 807, Taiwan, ROC
[b] Institute of Photonics and Communications, National Kaohsiung University of Applied Sciences, Kaohsiung, Taiwan, ROC

ARTICLE INFO

Article history:
Received 29 June 2009
Received in revised form
25 September 2009
Accepted 27 September 2009
Available online 9 October 2009

Keywords:
Phosphor
Activator
Photoluminescence
Sintering

ABSTRACT

This paper presents the characteristics of ZnS:Mn,Ce phosphor prepared by solid-state sintering. The luminance of ZnS:Mn phosphor was improved via energy transfer mechanism by co-doping with Ce sensitizer. XRD measurements show that the crystallization of ZnS:Mn,Ce is essentially dependent on the sintering temperature. The cubic- and hexagonal-ZnS phases coexisted at a sintering temperature of 900 °C. The content of the hexagonal-ZnS phase is increased with increasing sintering temperature, and a complete conversion to the hexagonal-ZnS phase occurs at 1200 °C. Photoluminescence analyses reveal that the emission peak of ZnS:Mn,Ce phosphor is red-shifted with increasing doping concentration, and is blue-shifted with increasing sintering temperature. Enhanced emission is induced in ZnS:Mn,Ce phosphor by indirect excitation, in which the electrons in the ZnS host and Ce sensitizer absorb the excitation energy and transfer it to the Mn activator for yellow emission.

1. Introduction

Recently, many researchers have investigated the optical properties of doped ZnS phosphors, particularly, Mn^{2+}-doped ZnS, because ZnS:Mn phosphors have potential applications in electroluminescence devices [1,2], field emission displays [3], and optical sensors [4]. However, for fabricating such devices, it is necessary to improve the luminescence of ZnS:Mn phosphors. Surface passivation is an efficient method for preparing ZnS:Mn phosphors, as it helps reduce the density of surface states, suppress non-radiative recombination, and stabilize the structural and optoelectronic properties of the phosphor [5–8]. Additionally, when nanocrystals are used to prepare such phosphor, the emission area is increased and quantum confinement occurs; because of this, the number of emission sites is increased and there is a great possibility of indirect transition at the crystal boundaries. This in turn results in enhanced absorption of excitation energy and improved luminescence characteristics [6,8]. Nevertheless, luminescence properties of nanocrystal phosphors are sensitive when there are changes in the environment; hence, an effective passivation layer is formed on the surface of the particles, because of which the luminescence properties of the phosphor are stabilized. The luminescence of nanocrystal phosphors can also be improved by irradiation treatment [9], thermal annealing [10], and optimization of doping concentration [11]. Energy transfer is another effective approach for enhancing the phosphor luminescence [12–16]. In recent years, extensive research has been carried out on resonant energy transfer among dopant ions in phosphors.

Co-doping processes have been carried out to prepare efficient ZnS:Mn phosphors that are based on energy transfer. In this method, an activator and a sensitizer with efficient excitation properties are doped into the host lattice. When the sensitizer and activator form small clusters in the host lattice, efficient energy transfer from the sensitizer to the activator takes place, and this results in enhanced luminescence [17–19]. In this case, the radiative lifetime of the sensitizer must be at least equal to that of the activator; otherwise, the sensitizer would decay instead of the activator, and this would result in undesired emission characteristics.

There are very few reports on the use of Mn and Ce as co-dopants for improving the luminance of sulfide phosphors, and the co-doping characteristics in this case have not been investigated in detail. Therefore, in this study, a yellow ZnS:Mn phosphor was prepared using Ce as the co-dopant to enhance the luminescence characteristics via energy transfer. The crystallization and luminescence properties of the ZnS:Mn,Ce phosphor are investigated.

2. Experimental

ZnS:Mn,Ce powder was synthesized using the conventional solid-state reaction method. First, the starting material ZnS (99.99%), MnO_2 (99.9%) and CeF_3 (99.9%) powders were mixed at a molar ratio of $ZnS:MnO_2:CeF_3 = 1:x:x$. The values of x were varied from 0.2 to 2.0, and the doping concentration of MnO_2 was equal to that of CeF_3. The source powders were then mixed with deionized water and milled for 24 h. Subsequently, the mixed solution was dried in an oven at a temperature of 80 °C for 8 h. The mixed powders were then sintered in a tube furnace at temperatures of

* Corresponding author. Tel.: +886 7 3814526; fax: +886 7 3811182.
E-mail address: shya@cc.kuas.edu.tw (S.-H. Yang).

0925-8388/$ – see front matter © 2009 Elsevier B.V. All rights reserved.
doi:10.1016/j.jallcom.2009.09.155

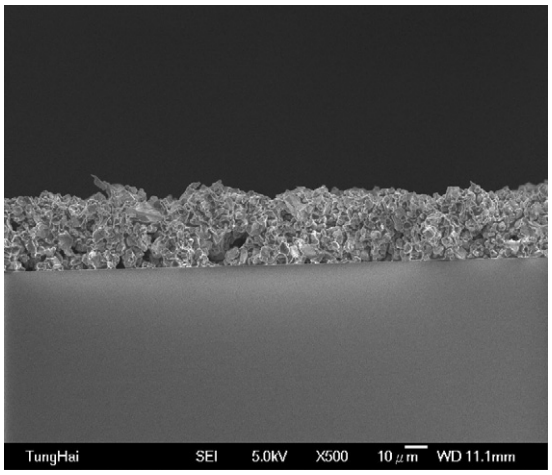

Fig. 1. Cross-sectional image of the phosphor film.

800–1000 °C for 1 h in a N_2 atmosphere. The flow rate of N_2 was set at 10 sccm. The redox reactions proceed during sintering. After sintering for 1 h, the ZnS:Mn,Ce phosphor was obtained.

In order to measure the luminescence property of the ZnS:Mn,Ce phosphor, phosphor films were prepared. An indium–tin oxide (ITO)-coated glass with a sheet resistance of 10 ohm per square was used as the substrate, and the phosphor was coated on ITO/glass by screen-printing to form the phosphor film. The weight ratio of polyvinyl alcohol binder to phosphor was 0.4. The printed phosphor film was subsequently dried naturally in air for 20 min, and then put into an oven and baked at 110 °C for 30 min to remove the binder. The film thickness estimated using a scanning electron microscope (SEM) was about 28 μm, as shown in Fig. 1.

A Hitachi F-4500 fluorescence spectrophotometer equipped with a 150 W xenon lamp and a monochrometer was used to evaluate the PL and PL excitation (PLE) spectra of the phosphor film. The excitation wavelength for PL measurement was set at 340 nm, scanning from 300 to 700 nm; the monitored wavelength for PLE analysis was fixed at 568 nm, the emission peak wavelength of phosphor. The surface morphology of the phosphor was evaluated with a JEOL 6330 TF field emission SEM operating at 5 kV. The element compositions were detected with an energy dispersive spectrometer (EDS), which was equipped in the SEM system. Furthermore, the crystalline phase was analyzed with a SIEMENS D5000 X-ray diffraction (XRD) system with Cu Kα radiation (λ = 0.1541 nm) and recorded in the range of $2\theta = 10–70°$ with an increment of 0.1°. For electroluminescence (EL) property measurements, the voltage was applied using a Keithley 2410 programmable voltage–current source, and the luminance and Commission Internationale de l'Eclairage (CIE) coordinates were measured using the Minolta chroma meter CS-100A.

3. Results and discussion

Fig. 2 shows the XRD patterns of ZnS:Mn,Ce phosphors doped with 0.9 mol% of MnO_2 and 0.9 mol% of CeF_3 and sintered for 1 h at different temperatures. This figure shows that the dominant structure of ZnS:Mn,Ce was cubic at 800 °C; C(1 1 1) was the main growth plane. No peaks corresponding to manganese and cerium compounds were observed, which demonstrates that the Mn and Ce ions were dispersed in the ZnS matrix and formed a solid solution. Co-existence of cubic and hexagonal ZnS:Mn,Ce occurred when the sintering temperature was 900 °C. When the sintering temperature increased, the ratio of hexagonal to cubic phases increased. The cubic ZnS:Mn,Ce was almost completely converted into the hexagonal phase at 1200 °C. The phase transition temperatures of the ZnS:Mn,Ce and ZnS were the same; the crystallization was essentially dependent on the sintering temperature. The XRD patterns of the ZnS:Mn,Ce phosphor sintered using different time and doping concentrations at 1200 °C were similar to Fig. 2(e). The weight ratio W_α/W_β of hexagonal ZnS (α-ZnS) to cubic ZnS (β-ZnS), determined by calculating the intensity ratio of the H(1 0 0) to C(2 0 0) diffraction peaks, can be expressed as follows [20]:

$$\frac{W_\alpha}{W_\beta} = 0.0968\frac{I_{H(100)}}{I_{C(200)}}. \quad (1)$$

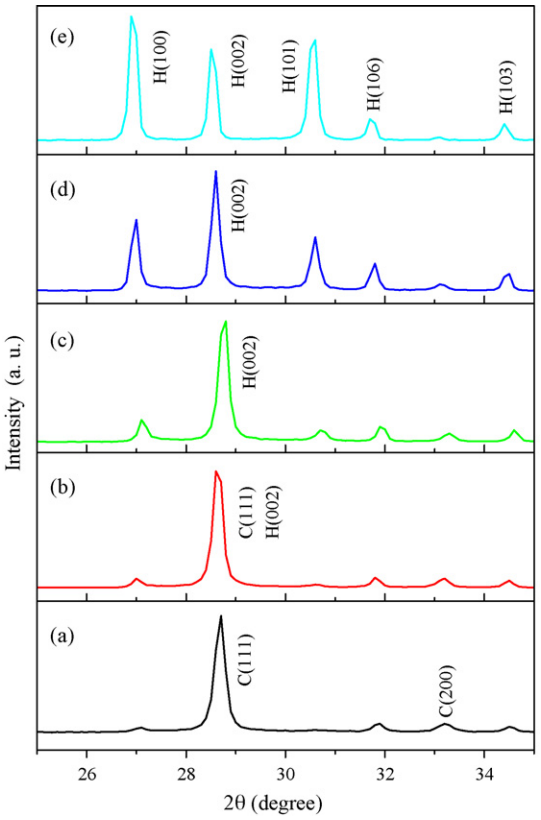

Fig. 2. XRD patterns of ZnS:Mn,Ce phosphors doped with 0.9 mol% of Mn and 0.9 mol% of Ce and sintered at different temperatures for 1 h: (a) 800 °C, (b) 900 °C, (c) 1000 °C, (d) 1100 °C, and (e) 1200 °C.

The proportion of the α-ZnS phase in the ZnS:Mn,Ce phosphor is

$$\%\alpha\text{-ZnS} = \frac{W_\alpha}{W_\alpha + W_\beta} \times 100\%. \quad (2)$$

Table 1 shows the proportion of the α-ZnS phase, the S/Zn atomic ratio, and the full width at half maximum (FWHM) of the α-ZnS (1 0 0) peak of the ZnS:Mn,Ce phosphor for different sintering conditions as obtained from XRD and EDS measurements. The proportion of the α-ZnS phase increased with increasing sintering temperature; however, it did not depend on the doping concentrations of Mn and Ce or on sintering time. The FWHM of H(1 0 0) shows that the crystallization of ZnS:Mn,Ce was improved by increasing the sintering temperature and time, but deteriorated in response to increasing doping concentrations. The mean particle size of the ZnS:Mn,Ce phosphor was approximately 38.9 nm when it was doped with 0.9 mol% of MnO_2 and 0.9 mol% of CeF_3 and sintered at 1200 °C for 1 h. The mean particle size was evaluated using the Debye–Scherrer formula, $D = 0.9\lambda/B\cos\theta$, where D is the particle size of phosphor, λ is the wavelength of X-ray radiation (0.154 nm), B is the FWHM (radian) and θ is the diffraction angle.

Fig. 3(a) shows the PLE spectra for the ZnS and ZnS:Mn,Ce phosphors, which were monitored at 568 nm, the emission peak wavelength of the ZnS:Mn,Ce phosphor; the ZnS:Mn,Ce phosphor was doped with 0.9 mol% of MnO_2 and 0.9 mol% of CeF_3. These spectra show that an excitation energy at wavelength approximately 340 nm was absorbed. For ZnS, the intrinsic absorption is at wavelength of 340 nm. However, when the monitored wavelength was at 568 nm, the intrinsic absorption of ZnS was low. On the contrary, the ZnS:Mn,Ce showed a relatively high absorption at wavelength 340 nm. Apparently, for the ZnS:Mn,Ce phosphor, the electrons in the ZnS host (bandgap = 3.67 eV) and Ce sensitizer

Table 1
Proportion of α-ZnS phase, S/Zn atomic ratio, and FWHM of the α-ZnS (1 0 0) peak of ZnS:Mn,Ce phosphor for different sintering conditions as obtained from XRD and EDS measurements.

Property	Sintering temperature (°C)					Sintering time (h)					Doping concentration (mol%)				
	800	900	1000	1100	1200	1	3	7	10	15	0.4	0.5	0.7	0.9	1.0
% α-ZnS	5.5	8.6	19.6	46.5	75.7	75.7	75.5	75.4	76.7	75.9	82.0	65.2	72.5	75.7	72.9
S/Zn	0.77	0.81	0.70	0.78	0.79	0.79	0.77	0.76	0.80	0.79	0.78	0.79	0.76	0.79	0.74
FWHM H(1 0 0)	0.23	0.23	0.22	0.21	0.21	0.21	0.21	0.22	0.19	0.20	0.20	0.20	0.21	0.21	0.22

absorbed the energy at wavelength 340 nm and underwent the band-edge and $4f^1 \rightarrow 5d^1$ transitions, respectively. The absorption of Ce^{3+} at wavelength of about 340 nm was reported by Leskelä et al. [21]. Furthermore, the PLE spectra monitored at 496 nm for the ZnS and ZnS:Mn,Ce phosphors are shown in Fig. 3(b). Inasmuch as the emission at wavelength of 496 nm was associated with sulfur vacancies of ZnS, therefore, a strong PLE peak related to intrinsic absorption of ZnS was observed. On the other hand, the absorption peak at wavelength of 340 nm was not found for ZnS:Mn,Ce when it was monitored at wavelength of 496 nm.

The PL spectra, for the ZnS:Mn,Ce phosphors doped with different concentrations of MnO_2 and CeF_3 and sintered at 1200 °C for 1 h, are shown in Fig. 4(a), where MnO_2 and CeF_3 were equal in doping concentration. The PL emission peak was at approximately 568 nm; it is associated with electron transition in $^4T_1$–$^6A_1$ of Mn^{2+} [22]. When the doping concentrations of MnO_2 and CeF_3 were less than 0.9 mol%, the PL intensity was substantially enhanced with increasing Mn^{2+} concentration. However, when the doping concentrations of MnO_2 and CeF_3 were more than 0.9 mol%, the emission from the ZnS:Mn,Ce phosphor decreased due to the concentration quenching effect. Moreover, it is observed that the emission peak was slightly red-shifted when increasing doping concentration. This was referred to the doping effect which introduces lattice distortion and ligand field decrease in ZnS:Mn,Ce, subsequently influencing the energy levels of Mn^{2+}. The optimal PL intensity was obtained when the ZnS phosphor was doped with 0.9 mol% of MnO_2 and 0.9 mol% of CeF_3.

Fig. 4(b) shows the PL spectra of ZnS:Mn,Ce phosphors doped with 0.9 mol% of MnO_2 and 0.9 mol% of CeF_3 and sintered at temperatures ranging from 800 to 1200 °C for 1 h. It was found that the change of ZnS:Mn,Ce from sphalerite to wurtize structure resulted in an enhancement in PL intensity and a blue-shifted emission; meanwhile, the improved crystallization of phosphor with increasing sintering temperature was another factor inducing variations in PL properties. The optimal sintering temperature, for achieving the maximum PL intensity of ZnS:Mn,Ce phosphor, was 1200 °C. However, PL spectra measurements showed that when the sintering time increased, the luminescence intensity of the phosphors was decreased by the increased particle size and the reduced emission area of the phosphor.

Fig. 4(c) shows the PL spectra of ZnS, ZnS:Mn (doped with 0.9 mol% of Mn) and ZnS:Mn,Ce (codoped with 0.9 mol% of MnO_2 and 0.9 mol% of CeF_3) phosphors sintered at 1200 °C for 1 h. As we know, the emission mechanisms of ZnS are related to surface/lattice defects, native impurities, sulfur vacancies V_S, zinc vacancies V_{Zn}, surface states and background impurity centers like Cu_{Zn} [23]. Here, V_S and V_{Zn} act as electron and hole traps, respectively. In this figure, the luminescence peak at 496 nm for ZnS was related to electron transfer from the V_S donor level to the background impu-

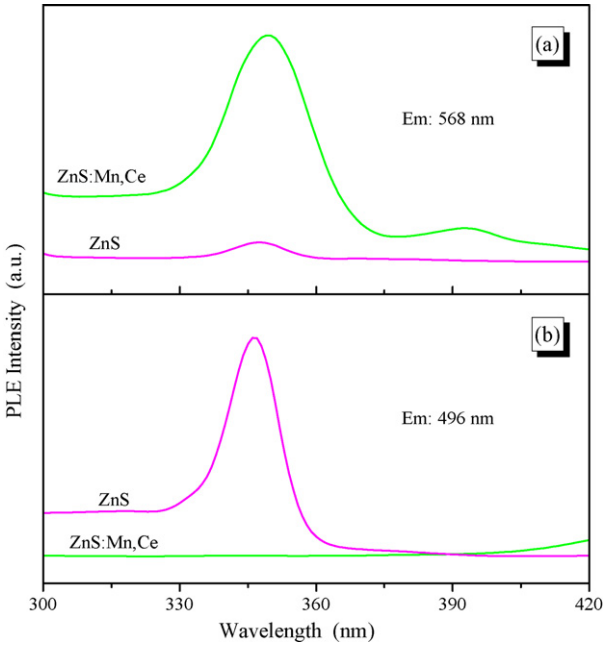

Fig. 3. PLE spectra for ZnS and ZnS:Mn,Ce phosphors monitored at wavelengths of (a) 568 nm and (b) 496 nm.

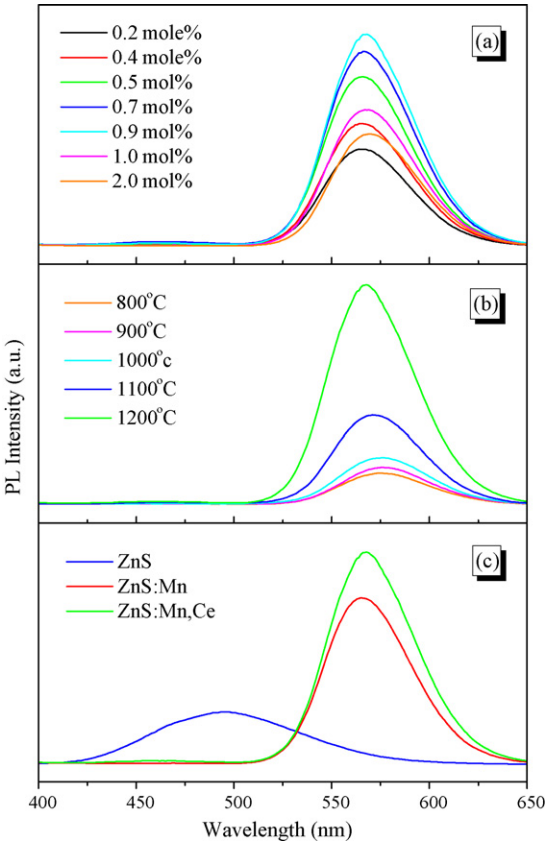

Fig. 4. PL spectra of ZnS:Mn,Ce phosphors (a) doped with different concentrations of MnO_2 and CeF_3 and sintered at 1200 °C for 1 h, (b) doped with 0.9 mol% of Mn and Ce and sintered at temperatures ranging from 800 to 1200 °C for 1 h, and (c) of ZnS, ZnS:Mn and ZnS:Mn,Ce (0.9 mol%) phosphors sintered at 1200 °C for 1 h.

rity centers. When Mn^{2+} ions are substituted for some Zn^{2+} ions in a ZnS crystal, the ^4G of the first excited state of Mn^{2+} in tetrahedral symmetry, T^d, is split. Thus the yellow PL peak at about 568 nm was associated with the $^4T_1$–$^6A_1$ transition of the Mn^{2+} ion in the ZnS tetrahedral lattice. Comparing the PL intensity of ZnS with ZnS:Mn phosphor, an improved luminescence intensity in the ZnS:Mn phosphor was measured due to the enhanced energy transfer from the ZnS host to the Mn activator. Furthermore, it was observed that the luminance intensity of the ZnS:Mn,Ce was higher than that of the ZnS:Mn phosphor due to the presence of the Ce^{3+} ions. Since the Mn^{2+} d–d transition is forbidden and difficult to pump, the emission of Mn^{2+} ions was indirectly excited by energy transfer from the ZnS host and the Ce^{3+} sensitizer; this is illustrated by Fig. 3(a), the PLE property of the ZnS:Mn,Ce phosphor. Because of the crystal-field disturbance, the effect of other ions around on the electronic structure of Mn^{2+} ions somewhat relieves the transition restriction. The intensified ZnS:Mn,Ce emission strongly supports ongoing energy transfer from the Ce^{3+} sensitizer to the Mn^{2+} activator. The energy is transferred from the ^5D level of the Ce^{3+} ion to the ^4G level of the Mn^{2+} ion by a process of resonance transfer via a spin exchange mechanism. Caldiño G reported that spectral overlap between $5d^1 \rightarrow 4f^1$ Ce^{3+} emission and $^6A_1 \rightarrow {}^4T_2$ Mn^{2+} absorption was measured [24,25]. McKeever et al. also reported that efficient pumping of the Mn^{2+} ion in CaF_2 can be achieved using the Ce^{3+} ion as sensitizer, and energy transfer mechanism took place in the Ce^{3+}–Mn^{2+} complex by using Dexter's theory [26]. In Fig. 4(c), the peak wavelength of PL spectrum of the ZnS:Mn was not changed by Ce doping, which reveals that Ce doping would not influence the multiplet energies of Mn^{2+}. Additionally, it is found that the emission of Ce^{3+} at wavelengths 450–600 nm for the ZnS:Mn,Ce phosphor was not observed, even though it was excited at wavelengths of 340 and 325 nm. Nevertheless, the emission of Ce^{3+}, excited at wavelength 340 nm, was observed from ZnS:Ce phosphor, as shown in Fig. 5. This emission spectrum can actually be fitted onto two Gaussian components by deconvolution. The emission peaks located at 496 and 545 nm were corresponded to V_S and Ce^{3+} emissions, respectively. Accordingly, it is expected that for the ZnS:Mn,Ce phosphor the absorption energy of Ce^{3+} was transferred to Mn^{2+}, as a result, an enhanced emission was measured.

In order to evaluate the luminance efficiency of the ZnS:Mn,Ce phosphor, an EL device with a structure of ITO/ZnS:Mn,Ce (10 μm)/$BaTiO_3$ (6 μm)/Ag was fabricated. The films were prepared by screen-printing, and the active area of the device was 5×10^{-2} cm^2. Fig. 6(a) shows the current–voltage and luminance–voltage curves of the device. The current and luminance of the device increased with applied voltage. The optimal luminance of 7.5 cd/m^2 was obtained at an applied voltage of 300 V and a current of 0.1 mA. Artlessness in the fabrication of the EL device was one of the causes of the low luminance efficiency. The CIE coordinates of the EL emission of the device were $x = 0.48$ and $y = 0.49$, as shown in Fig. 6(b); the EL emission image is displayed in the inset (applied voltage = 300 V).

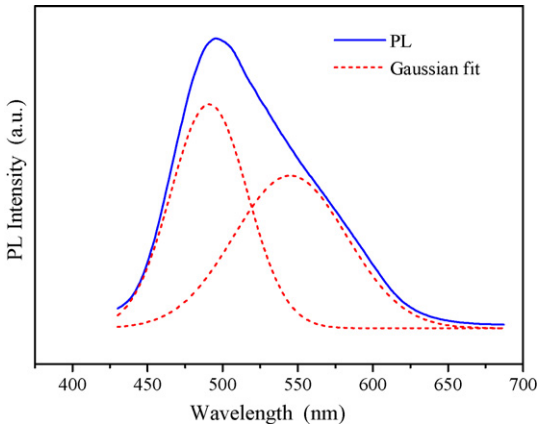

Fig. 5. PL spectrum of ZnS:Ce phosphor excited at wavelength of 340 nm. The Gaussian fit is shown as well.

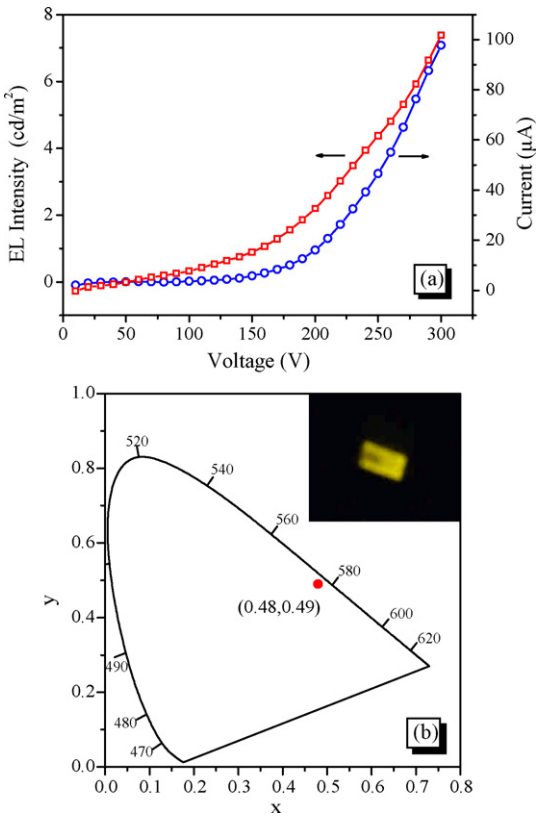

Fig. 6. (a) Current–voltage and luminance–voltage curves of the EL device, and (b) CIE coordinates of the device; the inset is the EL emission image.

4. Conclusions

An enhanced luminance of yellow ZnS:Mn,Ce phosphor was achieved via energy transfer mechanism and prepared by solid-state reaction. No XRD peaks corresponding to manganese and cerium compounds were observed, which demonstrates that the doped Mn and Ce ions were dissolved in the ZnS matrix. The crystallization of ZnS:Mn,Ce principally depended on the sintering temperature. The proportion of the α-ZnS phase was increased with increasing sintering temperature, which subsequently influenced the PL properties of the ZnS:Mn,Ce phosphor. PLE analyses revealed that emission from ZnS:Mn,Ce phosphor was induced by indirect excitation from the ZnS host and the Ce sensitizer, therefore an enhanced PL intensity was measured. However, the emission peak of the ZnS:Mn,Ce phosphor was shifted by increasing doping concentration and sintering temperature.

Acknowledgement

The authors would like to thank the National Science Council of the Republic of China, Taiwan, for financially supporting this research under contract No. NSC 97-2221-E-151-05.

References

[1] D.C. Koutsogeorgis, W.M. Cranton, R.M. Ranson, C.B. Thomas, J. Alloys Compd. 483 (2009) 526–529.

[2] D. Adachi, T. Morimoto, T. Hama, T. Toyama, H. Okamoto, J. Non-Cryst. Solids 354 (2008) 2740–2743.
[3] S.H. Shin, J.H. Kang, D.Y. Jeon, D.S. Zang, J. Solid State Chem. 178 (2005) 2205–2210.
[4] E. Mohagheghpour, M. Rabiee, F. Moztarzadeh, M. Tahriri, M. Jafarbeglou, D. Bizari, H. Eslami, Mater. Sci. Eng. C 29 (2009) 1842–1848.
[5] Y.T. Nien, K.H. Hwang, I.G. Chen, K. Yu, J. Alloys Compd. 455 (2008) 519–523.
[6] D.R. Jung, D. Son, J. Kim, C. Kim, B. Park, Appl. Phys. Lett. 93 (2008) 163118.
[7] A.K. Keshan, A.C. Pandey, J. Appl. Phys. 105 (2009) 064315.
[8] C.H. Lu, B. Bhattacharjee, S.Y. Chen, J. Alloys Compd. 475 (2009) 116–121.
[9] S. Chawla, N. Karar, H. Chander, Superlattice Microstruct. 43 (2008) 132–140.
[10] B. Steitz, Y. Axmann, H. Hofmann, A. Perri-Fink, J. Lumin. 128 (2008) 92–98.
[11] J. Cao, J. Yang, Y. Zhang, L. Yang, Y. Wang, M. Wei, Y. Liu, M. Gao, X. Liu, Z. Xie, J. Alloys Compd. (2009) 097, doi:10.1016/j.jallcom.2009.07.
[12] S. Yatsunenko, M. Godlewski, E. Guziewicz, M. Zalewska, A. Kłonkowski, M. Grinberg, P.J. Klar, W. Heimbrodt, J. Alloys Compd. 451 (2008) 206–208.
[13] M. Zalewska, S. Mahlik, B. Kukliński, M. Grinberg, A.M. Kłonkowski, Opt. Mater. 30 (2008) 719–721.
[14] S. Okamoto, K. Tanaka, Phys. Stat. Sol. C 3 (2006) 1059–1062.
[15] W. Chen, A.G. Joly, J.O. Malm, J.O. Bovin, J. Appl. Phys. 95 (2004) 667–672.
[16] H. Hu, W. Zhang, Opt. Mater. 28 (2006) 536–550.
[17] V. Singh, M. Tiwari, T.K.G. Rao, S.J. Dhoble, Bull. Mater. Sci. 28 (2005) 31–34.
[18] B. Wei, Z. lin, G. Wang, J. Cryst. Growth 295 (2006) 241–245.
[19] A. Nag, T.R.N. Kutty, Mater. Chem. Phys. 91 (2005) 524–531.
[20] Y.T. Nien, I.G. Chen, C.S. Hwang, S.Y. Chu, J. Electroceram. 17 (2006) 299–303.
[21] M. Leskelä, M. Tammenmaa, Mater. Chem. Phys. 16 (1987) 349–371.
[22] W.Q. Peng, S.C. Qu, G.W. Cong, X.Q. Zhang, Z.G. Wang, J. Cryst. Growth 282 (2005) 179–185.
[23] K. Manzoor, S.R. Vadera, N. Kumar, T.R.N. Kutty, Mater. Chem. Phys. 82 (2003) 718–725.
[24] U. Caldiño G, J. Phys.: Condens. Matter 15 (2003) 3821–3830.
[25] U. Caldiño G, J. Phys.: Condens. Matter 15 (2003) 7127–7137.
[26] S.W.S. McKeever, M.D. Brown, R.J. Abbundi, H. Chan, V.K. Mathur, J. Appl. Phys. 60 (1986) 2505–2510.